JACS
JOURNAL OF THE AMERICAN CHEMICAL SOCIETY
Communication
pubs.acs.org/JACS

# Three-Dimensional Graphene-Based Macro- and Mesoporous Frameworks for High-Performance Electrochemical Capacitive Energy Storage

Zhong-Shuai Wu,[†] Yi Sun,[†] Yuan-Zhi Tan,[†] Shubin Yang,[†] Xinliang Feng,*[,†,‡] and Klaus Müllen*[,†]

[†]Max-Planck-Institut für Polymerforschung, Ackermannweg 10, 55128 Mainz, Germany

[‡]School of Chemistry and Chemical Engineering, Shanghai Jiao Tong University, 200240 Shanghai, P.R. China

Supporting Information

**ABSTRACT:** Three-dimensional graphene-based frameworks (3D-GFs) with hierarchical macro- and mesoporous structures are presented. The interconnected macropores are derived from hydrothermally assembled 3D graphene aerogels (GAs), while the mesopores are generated by the silica networks uniformly grown on the surface of graphene. The resulting 3D-GFs exhibit narrow mesopore size distribution (2−3.5 nm), high surface area, and low mass density. These intriguing features render 3D-GFs a promising template for creating various 3D porous materials. Specifically, 3D GA-based mesoporous carbons (GA-MC) and metal oxide hybrids (GA-$Co_3O_4$, GA-$RuO_2$) can be successfully constructed via a nanocasting technology. Benefiting from the integration of meso- and macroporous structures, 3D GA-MC manifests outstanding specific capacitance (226 F $g^{-1}$), high rate capability, and excellent cycling stability (no capacitance loss after 5000 cycles) when it is applied in electrochemical capacitors.

Electrochemical capacitors (ECs) with high power density and excellent cycling stability are the crucial alternatives or supplements in energy storage devices that can meet the continuous energy demands and increasing environmental concerns.[1] Porous carbon materials such as activated carbon, carbide-derived carbon, ordered mesoporous carbons, carbon aerogels, and carbon nanotubes remain the most common and important electrode candidates for ECs.[2] To achieve fundamental insight into the electrode kinetic mechanisms and the correlation between porous structure of carbons and electrolyte ions,[3,4] considerable efforts have been devoted to fabricating high-performance ECs based on hierarchical porous carbons with macro-/meso-,[5] meso-/micro-,[6] macro-/micro-,[7] and macro-/meso-/micropores.[3,8] For these porous materials, the macropores can act as a bulk buffering reservoir for electrolytes to minimize the diffusion distances to the interior surfaces of the pores, while the mesopores can provide a large accessible surface area for ion transport/charge storage, and micropores can continuously increase charge accommodation. These features are desirable for applications in high-power ECs.[3,8]

Three-dimensional (3D) graphene-based frameworks (3D-GFs) such as aerogels, foams, and sponges are an important class of new-generation porous carbon materials, which exhibit continuously interconnected macroporous structures, low mass density, large surface area, and high electrical conductivity.[9] These materials can serve as robust matrix for accommodating metal, metal oxide, and electrochemically active polymers for various applications in ECs,[10,11] batteries,[12] and catalysis.[13] However, 3D-GFs generally lack well-defined mesopores and/or micropores, which substantially limits the efficiency of mass transport and charge storage for ECs through the small pores. Therefore, it is highly attractive to build up hierarchical porous architectures for 3D-GFs by integrating small mesoporous channels within interconnected macroporous frameworks.

Herein, we present the fabrication of hierarchical macro- and mesoporous 3D-GFs. Specifically, the interconnected macropores are derived from 3D graphene aerogels (GAs) that can be prepared by hydrothermal assembly of graphene oxide (GO), while the mesopores can be introduced by the silica networks uniformly grown on the graphene surface. The as-prepared 3D GA-based mesoporous silica composites (GA-$SiO_2$) exhibit tunable thickness of mesoporous silica walls, narrow mesopore size distribution (2−3.5 nm), interconnected macroporous networks, and low mass density. These features render the GA-$SiO_2$ a promising template for creating other 3D porous materials. For instance, 3D GA-based mesoporous carbon (GA-MC) and metal oxide (GA-$Co_3O_4$, GA-$RuO_2$) hybrids can be successfully constructed via a nanocasting technology.[14,15] Remarkably, 3D GA-MC shows outstanding specific capacitance (226 F $g^{-1}$), high rate capability, and excellent cycling stability (no capacitance loss after 5000 cycles) when it is applied in ECs, demonstrating a synergistic effect of macro- and mesopores.

The overall synthetic procedure leading to GA-$SiO_2$ is illustrated in Figure 1. First, GAs with high macroporosity and good mechanical properties (Figures S1−S3) were produced from hydrothermal assembly of GO in an aqueous suspension (1.5 mg $mL^{-1}$, Figure S4), followed by a freeze-drying process.[10] Afterward, the resulting monolithic GAs were immersed into a solution containing cetyltrimethylammonium bromide (CTAB), ethanol, NaOH, and deionized water.[14,15] Within this step, the surfactant cations ($CTA^+$) are expected to be electrostatically adsorbed and assembled on the negatively charged surface of GAs.[14,15] Subsequently, tetraethoxysilane

**Received:** August 31, 2012
**Published:** November 14, 2012

ACS Publications © 2012 American Chemical Society



dx.doi.org/10.1021/ja308676h | J. Am. Chem. Soc. 2012, 134, 19532−19535

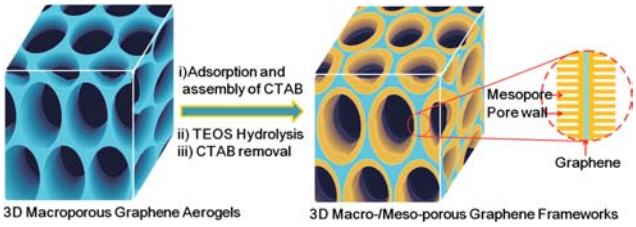


**Figure 1.** Fabrication of hierarchical macro- and mesoporous GA-$SiO_2$ frameworks: (i) electrostatic adsorption and assembly of CTAB on the surface of 3D GAs, (ii) TEOS hydrolysis for nucleation and growth of mesoporous silica on the surface of $CTA^+$-adsorped GAs, and (iii) CTAB removal through ethanol washing, drying, and thermal annealing.

(TEOS) was added as the silica source into the above mixture. During this process, TEOS would slowly hydrolyze and result in silica deposition on the surface of GAs. After washing with warm ethanol three times to remove CTAB surfactants, followed by drying and annealing at 800 °C for 3 h in $N_2$ gas, GA-$SiO_2$ was successfully constructed (see details in Supporting Information).

The morphology and microstructure of the as-prepared GA-$SiO_2$ were investigated by means of scanning electron microscopy (SEM), transmission electron microscopy (TEM), and nitrogen adsorption−desorption analysis. SEM images confirm that GA-$SiO_2$ possess 3D interconnected frameworks with randomly opened macroporous structure, similar to the original GAs (Figure 2a,b). The size of the

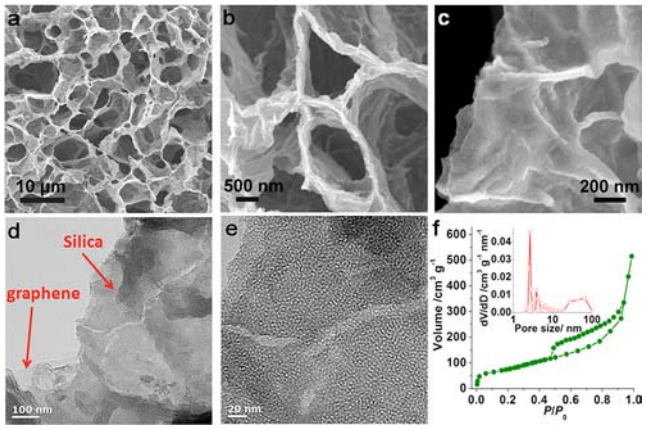


**Figure 2.** Morphology and microstructure of GA-$SiO_2$. (a) Low-magnification, (b) high-magnification, and (c) side-view SEM images of GA-$SiO_2$ reveal 3D macroporous interconnected frameworks and sandwich-like graphene−silica shells. (d) Representative TEM and (e) HRTEM images of GA-$SiO_2$ show sandwich-like graphene−silica shells with a mesoporous structure. (f) Isotherm plot and BJH pore distribution (inset) of GA-$SiO_2$ confirm the narrow mesopore size distribution (2.0−3.5 nm, pore size of ≥4.0 nm is from GAs) from the silica shells and a high BET surface area (350 $m^2$ $g^{-1}$).

macropores ranges from a few hundred nanometers to several micrometers. Different from GAs, GA-$SiO_2$ displays relatively rough surface morphology due to the presence of silica shells (Figure 2c), which have been uniformly grown on both sides of graphene in a sandwich-like manner (Figures 2d and S5). The typical thickness of silica walls is around 60−80 nm (Figure 2b), depending on the experimental conditions (Figures S6 and S7). Remarkably, a high-resolution TEM (HRTEM) image (Figure 2e) reveals that the resulting silica shells possess mesopores with a narrow size distribution of 2−3 nm. This result suggests that mesoporous silica was homogeneously nucleated and grown on 3D GAs.

The macro- and mesoporous feature of GA-$SiO_2$ was further confirmed by nitrogen adsorption−desorption measurements. The adsorption−desorption curve exhibits the prominent characteristic of type-IV isotherms with a distinct hysteresis loop of H2 in the $P/P_0$ range of 0.4−1.0, implying the presence of relatively large macropores and mesopores in the frameworks (Figure 2f). Moreover, the mesopore size calculated by the BJH method ranges from 2.0 to 3.5 nm with a narrow distribution (inset in Figure 2f). Brunauer−Emmett−Teller (BET) analysis reveals a specific surface area of 350 $m^2$ $g^{-1}$ and pore volume of 0.810 $cm^3$ $g^{-1}$ for GA-$SiO_2$, both of which are higher than those of GAs (220 $m^2$ $g^{-1}$ and 0.454 $cm^3$ $g^{-1}$, Figure S8). Element mapping images and energy-dispersive X-ray (EDX) analysis further unravel the homogeneous distribution of carbon, silicon, and oxygen in GA-$SiO_2$ (Figure 3). The weight percentage of

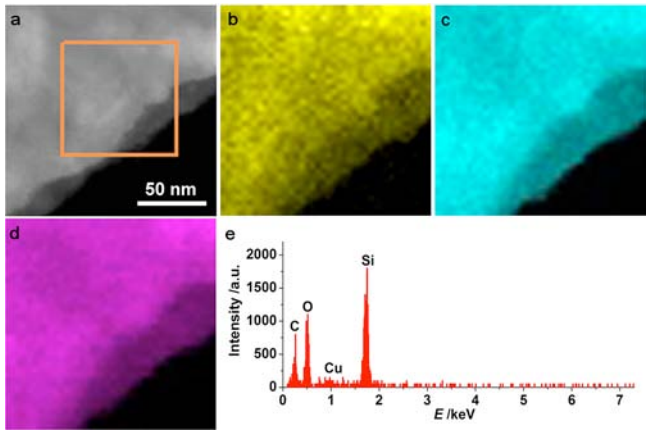


**Figure 3.** Elemental mapping images of GA-$SiO_2$. (a) Typical scanning transmission electron microscopy (STEM) image and corresponding elemental mapping images of (b) carbon, (c) silicon, and (d) oxygen in the selected area (orange rectangle in (a)), and (e) EDX spectrum suggest the homogeneous distribution of C, Si, and O in GA-$SiO_2$. The peak of Cu is from the copper TEM grid.

$SiO_2$ in GA-$SiO_2$ accessed by a thermogravimetry (TG) test is ∼53% (Figure S9). Therefore, these unique structural characteristics strongly suggest that GA-$SiO_2$ can serve as a template for generating porous materials with 3D interconnected macroporous networks and mesoporous channels. For instance, by choosing sucrose or cobalt (ruthenium) acetylacetonate as carbon or cobalt (ruthenium) source, novel 3D hybrids of GA-MC, GA-$Co_3O_4$, and GA-$RuO_2$ can be successfully synthesized, respectively (see details in Supporting Information).

Figure 4a−c shows the SEM and TEM images of GA-MC. Apparently, SEM images (Figure 4a,b) reveal that GA-MC possesses a similar morphology as the original 3D GAs, which are featured by fully interconnected macroporous frameworks. The XRD pattern (Figure S10) indicates the amorphous nature of porous carbon for GA-MC. TEM (Figure S11) and HRTEM (Figure 4c) images clearly show the presence of mesopores in the carbon walls with a size of 2−3 nm, indicating the successful replication of the structure from GA-$SiO_2$ into GA-MC. A BET specific surface area of up to 295 $m^2$ $g^{-1}$ can be obtained based on the nitrogen adsorption−desorption analysis. Similarly, the pore size distribution further demonstrates the existence of a


dx.doi.org/10.1021/ja308676h | J. Am. Chem. Soc. 2012, 134, 19532−19535

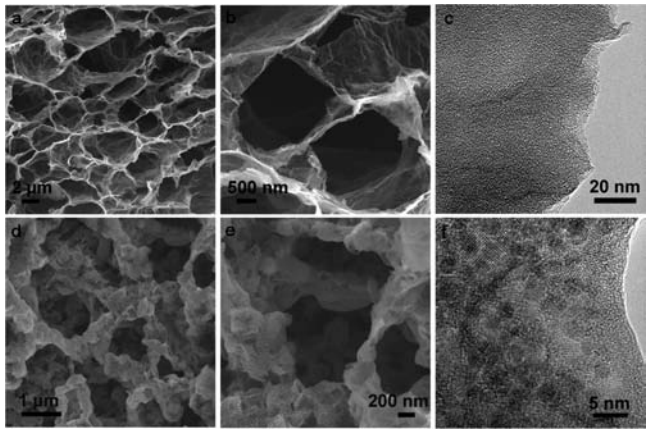


**Figure 4.** 3D GA-MC and GA-$Co_3O_4$ materials derived from the as-prepared GA-$SiO_2$. (a,b) SEM and (c) HRTEM images of GA-MC reveal the mesoporous structure of the walls and macroporous interconnected framework. (d,e) SEM images of GA-$Co_3O_4$ demonstrate the macroporous structure with increased thickness of the frameworks. (f) HRTEM images of GA-$Co_3O_4$ disclose the uniform distribution of ultrasmall (2−3 nm) crystalline nanoparticles of $Co_3O_4$ on graphene sheets.

large number of mesopores (2.0−3.5 nm) and macropores in GA-MC (Figure S12).

Given the unique porous features for GA-MC, we further evaluated its electrochemical performance as electrode for ECs in a three-electrode system, applying 1 M $H_2SO_4$ as electrolyte, as shown in Figure 5. The cyclic voltammetry (CV) profiles exhibit a typical electrical double layer behavior at all sweeping rates (Figure 5a) and the specific capacitance obtained at 1 mV $s^{-1}$ is about ~226 F $g^{-1}$. This value is much higher than that of the macroporous GAs (~176 F $g^{-1}$), mesoporous carbon (MC, 143 F $g^{-1}$) without involving graphene (see Supporting Information), physically mixed GA-MC with a 1:1 weight ratio (~158 F $g^{-1}$), two-dimensional graphene-based mesoporous carbon sheets[14] (GMC, 148 F $g^{-1}$) without macropores (see Supporting Information), and reduced graphene powder (146 F $g^{-1}$) (Figure 5b) for ECs. These parallel experiments on different graphene-based carbon materials strongly suggest the critical importance of integrating mesopores into macroporous frameworks to improve the electrochemical performance. Thereby, a synergistic effect of macro- and mesopores is validated (Figure S13): (i) The interconnected macropores within frameworks are favorable for buffering ions to shorten the diffusion distances from the external electrolyte to the interior surfaces. (ii) The mesopores in thin walls, together with the presence of micropores derived from the stacked graphene layers, can enhance ion transport and charge storage.[3,16] (iii) The conductive graphene sheets within 3D frameworks can serve as multidimensional pathways to facilitate the transport of electrons in the bulk electrode.[10,11]

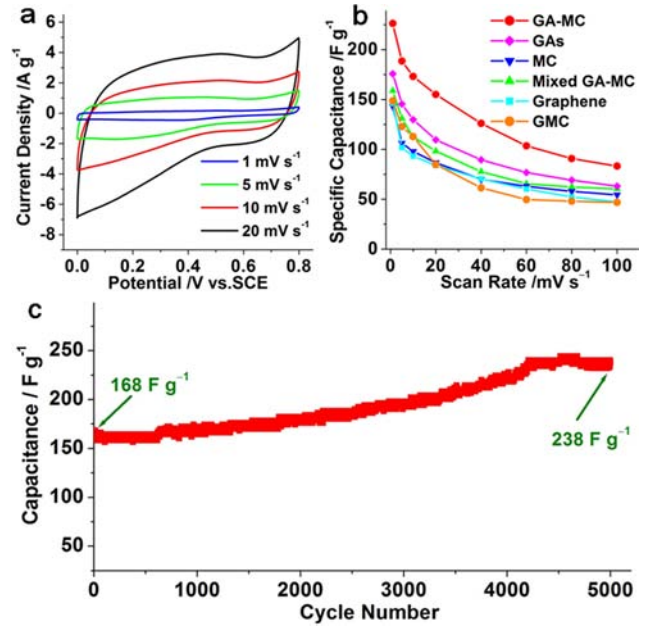


**Figure 5.** Electrochemical performance of GA-MC electrode for ECs. (a) CVs of GA-MC electrode measured at different scan rates in 1 M $H_2SO_4$ electrolyte. (b) Specific capacitance as a function of scan rates for GA-MC, GAs, MC, mixed GA-MC, 2D GMC, and graphene powder electrodes. (c) Cycling stability of GA-MC electrode for ECs, measured at 2 A $g^{-1}$ in 1 M $H_2SO_4$ electrolyte.

Furthermore, GA-MC displays good capacitance retention (Figure 5b). For instance, a highest specific capacitance of ~83 F $g^{-1}$ was obtained among our measured samples at a high scan rate of 100 $mVs^{-1}$, demonstrating the reduced ion transport limitation in macro-/mesoporous 3D materials. The cycling stability of GA-MC was also evaluated by galvanostatic charge−discharge measurement at 2 A $g^{-1}$ in 1 M $H_2SO_4$ electrolyte. Remarkably, no capacitance loss was observed for GA-MC after 5000 cycles (Figure 5c). The enhanced capacity may be attributed to the improvement of ion accessibility in 3D graphene frameworks during the cycling process which leads to an increased accommodation behavior for charges.

On the other hand, GA-$SiO_2$ is also a promising template for fabricating novel 3D graphene/metal oxide hybrids for electrochemical energy storage and conversion systems. For instance, GA-$Co_3O_4$ hybrids were prepared by infiltration of the as-prepared GA-$SiO_2$ into 2-isopropanol solution containing cobalt acetylacetonate, followed by heating at 350 °C for 3 h in air, and NaOH etching of mesoporous silica. Figure 4d−f shows the SEM and TEM characterizations for GA-$Co_3O_4$. Obviously, GA-$Co_3O_4$ hybrids possess 3D interconnected macroporous frameworks (Figure 4d,e), associated with mesoporous and crystalline structures of $Co_3O_4$ (Figure 4f). Interestingly, ultrasmall $Co_3O_4$ nanoparticles with a size of 2−3 nm are uniformly deposited on the surface of 3D GAs (Figures 4f and S14). The pure phase of $Co_3O_4$ in hybrids was revealed by the XRD pattern (Figure S15). This result suggests that $Co_3O_4$ nanoparticles were confined in the mesopores of the silica template during the fabrication process. The presence of graphene and $Co_3O_4$ in GA-$Co_3O_4$ was further confirmed by XPS analysis (Figure S16). Similarly, this synthetic strategy was used to fabricate 3D GA-$RuO_2$ hybrids (~42 wt% $RuO_2$) (Figure S17). Due to the decoration of uniform and ultrasmall $RuO_2$ nanoparticles (~2 nm) on 3D GAs, the resulting hybrids exhibit high specific capacitance (560 F $g^{-1}$) for ECs. Importantly, the pseudocapacitive utilization of $RuO_2$ in hybrid is as high as ~1090 F $g^{-1}$ (Figure S18), which is comparable to the best reported values.[17]

In summary, we have successfully integrated mesoporous silica walls within 3D interconnected macroporous graphene-based frameworks. The resulting GA-$SiO_2$ possess macro- and mesoporous structures with a high specific surface area, enabling the construction of other graphene-based materials with hierarchical porous features. The fabricated 3D graphene-


dx.doi.org/10.1021/ja308676h | J. Am. Chem. Soc. 2012, 134, 19532−19535

based mesoporous carbon and metal oxide materials show enhanced supercapacitive performance, such as high specific capacitance, good rate capability, and excellent cycling stability. By adjusting the shell thickness and the mesopore size, we believe that our approach can provide a variety of new 3D hierarchical porous materials for the application in a broad range of ECs, batteries, sensors, catalysis, adsorbents, and fuel cells.

## ■ ASSOCIATED CONTENT

### Supporting Information

Full synthesis and characterization details; AFM image of GO; SEM, mercury-intrusion porosimetry, mechanical properties, and nitrogen cryosorption isotherm of GAs; TEM, SEM, and TG of GA-$SiO_2$; XRD, TEM, nitrogen cryosorption isotherm of GA-MC, and schematic representation of macropores and mesopores for ECs; TEM, HRTEM, XRD, and XPS of GA-$Co_3O_4$; and SEM, TEM, HRTEM images, and CVs of GA-$RuO_2$. This material is available free of charge via the Internet at http://pubs.acs.org.

## ■ AUTHOR INFORMATION

### Corresponding Author

feng@mpip-mainz.mpg.de; muellen@mpip-mainz.mpg.de

### Notes

The authors declare no competing financial interest.

## ■ ACKNOWLEDGMENTS

The authors thank Prof. Dr. X. H. Wang and Prof. Dr. F. Li for the help with mercury-intrusion porosimetry measurement and X. Deng and M. Ye for testing mechanical properties. Financial support by the ERC grants on NANOGRAPH, 2DMATER, ENERCHEM, DFG Priority Program SPP 1459, BMBF LiBZ, ESF Project GOSPEL (ref. no. 9-EuroGRAPHENE-FP-001), EU Project GENIUS, and MOLESOL.

## ■ REFERENCES

(1) (a) Chmiola, J.; Yushin, G.; Gogotsi, Y.; Portet, C.; Simon, P.; Taberna, P. L. *Science* **2006**, *313*, 1760. (b) Simon, P.; Gogotsi, Y. *Nat. Mater.* **2008**, *7*, 845. (c) Miller, J. R.; Simon, P. *Science* **2008**, *321*, 651. (d) Chmiola, J.; Largeot, C.; Taberna, P. L.; Simon, P.; Gogotsi, Y. *Science* **2010**, *328*, 480. (e) El-Kady, M. F.; Strong, V.; Dubin, S.; Kaner, R. B. *Science* **2012**, *335*, 1326.

(2) (a) Zhai, Y. P.; Dou, Y. Q.; Zhao, D. Y.; Fulvio, P. F.; Mayes, R. T.; Dai, S. *Adv. Mater.* **2011**, *23*, 4828. (b) Gao, W.; Singh, N.; Song, L.; Liu, Z.; Reddy, A. L. M.; Ci, L. J.; Vajtai, R.; Zhang, Q.; Wei, B. Q.; Ajayan, P. M. *Nature Nanotechnol.* **2011**, *6*, 496. (c) Zhu, Y. W.; Murali, S.; Stoller, M. D.; Ganesh, K. J.; Cai, W. W.; Ferreira, P. J.; Pirkle, A.; Wallace, R. M.; Cychosz, K. A.; Thommes, M.; Su, D.; Stach, E. A.; Ruoff, R. S. *Science* **2011**, *332*, 1537. (d) Guo, B. K.; Wang, X. Q.; Fulvio, P. F.; Chi, M. F.; Mahurin, S. M.; Sun, X. G.; Dai, S. *Adv. Mater.* **2011**, *23*, 4661.

(3) Wang, D. W.; Li, F.; Liu, M.; Lu, G. Q.; Cheng, H. M. *Angew. Chem., Int. Ed.* **2008**, *47*, 373.

(4) (a) Largeot, C.; Portet, C.; Chmiola, J.; Taberna, P. L.; Gogotsi, Y.; Simon, P. *J. Am. Chem. Soc.* **2008**, *130*, 2730. (b) Merlet, C.; Rotenberg, B.; Madden, P. A.; Taberna, P. L.; Simon, P.; Gogotsi, Y.; Salanne, M. *Nat. Mater.* **2012**, *11*, 306.

(5) (a) Wang, Z. Y.; Stein, A. *Chem. Mater.* **2008**, *20*, 1029. (b) Li, F. J.; Morris, M.; Chan, K. Y. *J. Mater. Chem.* **2011**, *21*, 8880.

(6) (a) Raymundo-Pinero, E.; Cadek, M.; Beguin, F. *Adv. Funct. Mater.* **2009**, *19*, 1032. (b) Rose, M.; Korenblit, Y.; Kockrick, E.; Borchardt, L.; Oschatz, M.; Kaskel, S.; Yushin, G. *Small* **2011**, *7*, 1108.

(7) (a) Backov, R. *Soft Matter* **2006**, *2*, 452. (b) Brun, N.; Prabaharan, S. R. S.; Morcrette, M.; Sanchez, C.; Pecastaings, G.; Derre, A.; Soum, A.; Deleuze, H.; Birot, M.; Backov, R. *Adv. Funct. Mater.* **2009**, *19*, 3136. (c) Gutierrez, M. C.; Pico, F.; Rubio, F.; Amarilla, J. M.; Palomares, F. J.; Ferrer, M. L.; del Monte, F.; Rojo, J. M. *J. Mater. Chem.* **2009**, *19*, 1236.

(8) (a) Hasegawa, G.; Aoki, M.; Kanamori, K.; Nakanishi, K.; Hanada, T.; Tadanaga, K. *J. Mater. Chem.* **2011**, *21*, 2060. (b) Jiang, H.; Ma, J.; Li, C. Z. *Adv. Mater.* **2012**, *30*, 4197. (c) Brun, N.; Prabaharan, S. R. S.; Surcin, C.; Morcrette, M.; Deleuze, H.; Birot, M.; Babot, O.; Achard, M. F.; Backov, R. *J. Phys. Chem. C* **2012**, *116*, 1408.

(9) (a) Worsley, M. A.; Pauzauskie, P. J.; Olson, T. Y.; Biener, J.; Satcher, J. H.; Baumann, T. F. *J. Am. Chem. Soc.* **2010**, *132*, 14067. (b) Xu, Y. X.; Wu, Q. O.; Sun, Y. Q.; Bai, H.; Shi, G. Q. *ACS Nano* **2010**, *4*, 7358. (c) Tang, Z. H.; Shen, S. L.; Zhuang, J.; Wang, X. *Angew. Chem., Int. Ed.* **2010**, *49*, 4603. (d) Lee, S. H.; Kim, H. W.; Hwang, J. O.; Lee, W. J.; Kwon, J.; Bielawski, C. W.; Ruoff, R. S.; Kim, S. O. *Angew. Chem., Int. Ed.* **2010**, *49*, 10084. (e) Chen, Z. P.; Ren, W. C.; Gao, L. B.; Liu, B. L.; Pei, S. F.; Cheng, H. M. *Nat. Mater.* **2011**, *10*, 424.

(10) Wu, Z. S.; Winter, A.; Chen, L.; Sun, Y.; Turchanin, A.; Feng, X.; Müllen, K. *Adv. Mater.* **2012**, *24*, 5130.

(11) (a) Choi, B. G.; Yang, M.; Hong, W. H.; Choi, J. W.; Huh, Y. S. *ACS Nano* **2012**, *6*, 4020. (b) Cao, X. H.; Shi, Y. M.; Shi, W. H.; Lu, G.; Huang, X.; Yan, Q. Y.; Zhang, Q.; Zhang, H. *Small* **2011**, *7*, 3163. (c) Dong, X. C.; Xu, H.; Wang, X. W.; Huang, Y. X.; Chan-Park, M. B.; Zhang, H.; Wang, L. H.; Huang, W.; Chen, P. *ACS Nano* **2012**, *6*, 3206.

(12) (a) Xiao, J.; Mei, D. H.; Li, X. L.; Xu, W.; Wang, D. Y.; Graff, G. L.; Bennett, W. D.; Nie, Z. M.; Saraf, L. V.; Aksay, I. A.; Liu, J.; Zhang, J. G. *Nano Lett.* **2011**, *11*, 5071. (b) Chen, W. F.; Li, S. R.; Chen, C. H.; Yan, L. F. *Adv. Mater.* **2011**, *23*, 5679.

(13) (a) Wu, Z. S.; Yang, S. B.; Sun, Y.; Parvez, K.; Feng, X. L.; Müllen, K. *J. Am. Chem. Soc.* **2012**, *134*, 9082. (b) Yong, Y. C.; Dong, X. C.; Chen-Park, M. B.; Song, H.; Chen, P. *ACS Nano* **2012**, *6*, 2394.

(14) Yang, S. B.; Feng, X. L.; Wang, L.; Tang, K.; Maier, J.; Müllen, K. *Angew. Chem., Int. Ed.* **2010**, *49*, 4795.

(15) (a) Yang, S. B.; Feng, X. L.; Wang, X. C.; Müllen, K. *Angew. Chem., Int. Ed.* **2011**, *50*, 5339. (b) Yang, S. B.; Feng, X. L.; Müllen, K. *Adv. Mater.* **2011**, *23*, 3575.

(16) Fan, L. Z.; Hu, Y. S.; Maier, J.; Adelhelm, P.; Smarsly, B.; Antonietti, M. *Adv. Funct. Mater.* **2007**, *17*, 3083.

(17) (a) Zheng, J. P.; Cygan, P. J.; Jow, T. R. *J. Electrochem. Soc.* **1995**, *142*, 2699. (b) Zhang, J. R.; Jiang, D. C.; Chen, B.; Zhu, J. J.; Jiang, L. P.; Fang, H. Q. *J. Electrochem. Soc.* **2001**, *148*, A1362. (c) Kim, I. H.; Kim, J. H.; Lee, Y. H.; Kim, K. B. *J. Electrochem. Soc.* **2005**, *152*, A2170.